Ann. Geophys., 28, 1013–1021, 2010
www.ann-geophys.net/28/1013/2010/

Annales Geophysicae

Source mechanism of Saturn narrowband emission

J. D. Menietti[1], P. H. Yoon[2,3], Sheng-Yi Ye[1], B. Cecconi[4], and A. M. Rymer[5]

[1]Dept. of Physics and Astronomy, University of Iowa, Iowa City, IA, USA
[2]Institute for Physical Science and Technology, University of Maryland, College Park, MD, USA
[3]School of Space Research, Kyung Hee University, Yongin, Gyeonggi 446-701, Korea
[4]LESIA-CNRS, Observatoire de Paris, Meudon, France
[5]Applied Physics Laboratory, Johns Hopkins University, Laurel, MD, USA

Received: 23 August 2009 – Revised: 22 March 2010 – Accepted: 18 April 2010 – Published: 27 April 2010

Abstract. Narrowband emission (NB) is observed at Saturn centered near 5 kHz and 20 kHz and harmonics. This emission appears similar in many ways to Jovian kilometric narrowband emission observed at higher frequencies, and therefore may have a similar source mechanism. Source regions of NB near 20 kHz are believed to be located near density gradients in the inner magnetosphere and the emission appears to be correlated with the occurrence of large neutral plasma clouds observed in the Saturn magnetotail. In this work we present the results of a growth rate analysis of NB emission (∼20 kHz) near or within a probable source region. This is made possible by the sampling of in-situ wave and particle data. The results indicate waves are likely to be generated by the mode-conversion of directly generated Z-mode emission to O-mode near a density gradient. When the local hybrid frequency is close $n\ f_{ce}$ (n is an integer and f_{ce} is the electron cyclotron frequency) with n=4, 5 or 6 in our case, electromagnetic Z-mode and weak ordinary (O-mode) emission can be directly generated by the cyclotron maser instability.

Keywords. Magnetospheric physics (Plasma waves and instabilities)

1 Introduction

Earth orbiting satellites have revealed two general types of non-thermal emission: directly generated emission and mode-converted (indirect) emission. Auroral kilometric radiation (AKR) is one of the most intense terrestrial radio emissions and is directly generated by the cyclotron maser instability (Wu and Lee, 1979). Terrestrial continuum emission and narrowband radio emissions are believed to be generated indirectly by mode conversion from intense electrostatic waves (Gurnett, 1975; Jones, 1976; Melrose, 1981). Jovian decametric emission and Saturn kilometric radiation (SKR) are believed to be directly generated by the cyclotron maser instability and are therefore counterparts of terrestrial AKR. Similarly, narrowband radio emissions present at Jupiter (narrowband kilometric emission or nKOM) and at Saturn (narrowband emission) with similar characteristics to terrestrial narrowband continuum emission are believed to have a similar source mechanism (cf. Louarn et al., 2007).

The source mechanism of continuum emission and planetary non-thermal continuum emission has been proposed to be a mode conversion process occurring near the dayside magnetopause and/or the night side plasmapause near the equator. Both linear (e.g. Jones, 1976, 1988; Budden, 1980) and nonlinear (cf. Melrose, 1981; Barbosa, 1982; Fung and Papadopoulos, 1987; Ronnmark, 1983) classes of mode conversion have been suggested as summarized in Kurth (1992). All of these mechanisms involve electrostatic upper hybrid waves. In the linear mechanism upper hybrid waves refract (in a steep density gradient) to Z-mode waves at a wave normal angle near 90°. Z-mode waves can mode convert to O-mode waves (cf. Horne, 1989; 1990). The nonlinear mechanisms are described by the authors as more efficient than the linear conversion mechanism (Ronnmark, 1989, 1992). For these processes electrostatic upper hybrid waves coalesce with some lower frequency wave.

Electrostatic $(n+1/2)\,f_{ce}$ waves near f_{UH} (f_{ce} is the electron cyclotron frequency and f_{UH} is the upper hybrid frequency) are frequently observed in space plasmas and are often found to be associated with observation of loss cone electron distribution at the source (Kurth et al., 1979a, b). Ronnmark et al. (1978) has shown that wave growth rate maximizes when $(n+1/2)\,f_{ce} \sim f_{UH}$ due to the nonconvective

Correspondence to: J. D. Menietti
(john-menietti@uiowa.edu)

Published by Copernicus Publications on behalf of the European Geosciences Union.

nature of the instability. Auroral roar emission is left-hand ordinary (L-O) mode emission observed by ground-based receivers at frequencies from ∼0.03–30 MHz. Narrowband emissions are interpreted as emissions near the first and second harmonics of f_{ce}. In explaining the generation of terrestrial auroral roar, Yoon et al. (1996, 1998) have shown that the growth rates of Z-mode are greatly enhanced when $f_{UH}^2 = f_{ce}^2 + f_p^2 = (nf_{ce})^2$, where n=2 and 3 (f_p is the electron plasma frequency). This Z-mode can escape into free space by a linear mode conversion into ordinary (O) or whistler mode (e.g. Ellis, 1956).

The first detections of narrowband radio emission from Saturn were made by Voyager (Gurnett et al., 1981; Scarf et al., 1982). Voyager 1 observed a band of emission near 5 kHz between about 3.25 R_S and 58 R_S. Ye et al. (2009) have recently presented an extensive survey of narrowband emissions observed in the Saturn magnetosphere by the Cassini RPWS instrument, primarily at frequencies near 5 kHz and near 20 kHz and sometimes harmonics separated by the local cyclotron frequency, f_{ce}. The emission is observed most intensely associated with storms of Saturn kilometric radiation and then is seen in each rotation. The typical bandwidth is 1–3 kHz. Ye et al. (2009) have identified the electromagnetic emission as ordinary (O) mode. They present direction finding results supported with observations that locate the sources of the 20 kHz emission off the magnetic equator near the intersection of the surface of f_{ce} and the surface of plasma frequency where $(n+1/2)\, f_{ce} \sim f_{UH}$. The emissions originate from the northern and southern edges of Saturn's plasma torus at $L \sim 7$ to 10 for 5 kHz or $L \sim 4$ to 7 for 20 kHz emission (L is determined assuming a Saturn-centered dipole magnetic field). These locations are consistent with the hypothesis that the emission is similar to continuum emission observed at Earth (cf. Gurnett and Shaw, 1973; Morgan and Gurnett, 1991) and at Jupiter (Gurnett et al., 1983). Wang et al. (2009) summarized the observations of narrowband radio emissions by Cassini and examined the possible association of narrowband radio emissions with a revolving plasma cloud detected by the MIMI/INCA (Magnetospheric Imaging/Ion and Neutral Camera) instrument onboard Cassini.

Menietti et al. (2009) analyzed an example of NB emission near a possible source region in the mid-latitude Southern Hemisphere of Saturn. In situ electron distributions suggest NB has a source region associated with electrostatic cyclotron and upper hybrid emission. Linear growth rate calculations indicate that the observed plasma distributions are unstable to the growth of electrostatic harmonic emissions. In addition, it is found that when the local hybrid frequency is close to 3 f_{ce} (f_{ce} is the electron cyclotron frequency), electromagnetic Z-mode and weak ordinary (O-mode) emission are directly generated by the cyclotron maser instability. In the presence of density gradients observed near the purported source region, Z-mode emission can mode-convert into O-mode emission, and Menietti et al. (2009) suggested that this might explain the NB emission observed by the Cassini spacecraft. These authors noted that it will be important to test this scenario for other encounters with source regions of NB, especially for conditions of varying ratios of $f_{p/}\, f_{ce}$.

Ye et al. (2009) present a list of 20 possible source regions of "20 kHz narrowband source encounter events" (cf. their Table 1). In this table the events vary over a range of parameters $2.76\, R_S < r < 7.75\, R_S$, -31.2° <Latitude< 25.3°, and 16.8 h<Local Time<4.8 h (where the latter extends through midnight). While there is uncertainty in many values of f_{uh}, the ratio of f_p/f_{ce} varies from close to 1 to as high as 17 in one case. The emission frequencies vary from about 10 kHz to about 35 kHz.

In this paper we examine in some detail new examples of NB observed by Cassini at Saturn with center frequency near 15 kHz. The examples are associated with electrostatic cyclotron harmonic (ECH) emission and probable upper hybrid waves, similar to the case examined by Menietti et al. (2009), but in this new case, the source is in the Northern Hemisphere and the ratio of f_p/f_{ce} appears to be somewhat higher. We conduct a similar analysis of the in-situ wave and particle data, including a spatial growth calculation, to demonstrate that the cyclotron maser instability is likely responsible for the direct generation of Z-mode emission which may mode convert to O mode or NB emission as observed.

2 Observations and wave growth rate analysis

As explained in Ye et al. (2009) the Saturn NB emissions observed most frequently near 20 kHz have source regions that probably lie on the northern and southern edges of the plasma density torus at Saturn. These are best observed during Cassini orbits that extend to higher latitudes.

We have obtained electron phase space density data for 14 of the 20 cases in Table 1 of Ye et al. (2009). Of these 14, only 2 cases have sufficient pitch angle distribution and circular polarization data for further analyses: day 269 of 2006 and day 003 of 2008. The physical location and plasma parameters for these two events are quite similar. We have chosen day 003 of 2008 for detailed study because it had comparatively more temporal stability. At the time the spacecraft was at a northern latitude of about 23 degrees, proceeding southward at a radial distance of about 6 R_S at a local time of about 21:00.

In Fig. 1 we display the wave spectrogram for day 003 of 2008 for the time interval 16:30 to 22:00 UT. The frequency axis is linear ranging from 1 kHz to 90 kHz. The white line near the bottom of the plot indicates f_{ce}, and the increasing upper hybrid emission, f_{UH}, indicated with an arrow, indicates a steep density gradient. Narrowband emission indicated by arrows emanates from possible source regions near 17:30 and 19:00 where intense oscillations of the electric field are observed. In Fig. 2 we show a close up of the probable source region of NB, indicating the bandwidth of intense emission extends from about 10 kHz to over 17 kHz.

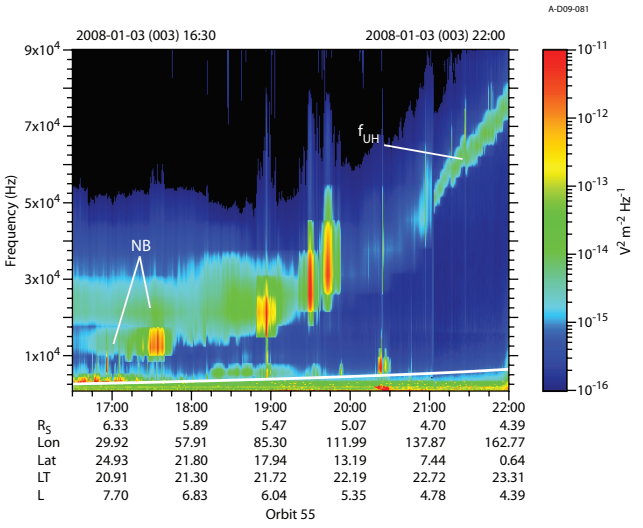

Fig. 1. A frequency versus time wave spectrogram for day 003 of 2008 for the time interval 16:30 to 22:00 UT. The frequency axis is linear ranging from 1 to 90 kHz. The white line near the bottom of the plot indicates f_{ce}, and upper hybrid resonance emission is indicated with an arrow. Narrowband emission, indicated by arrows, emanates from possible source regions near 17:30 and 19:00.

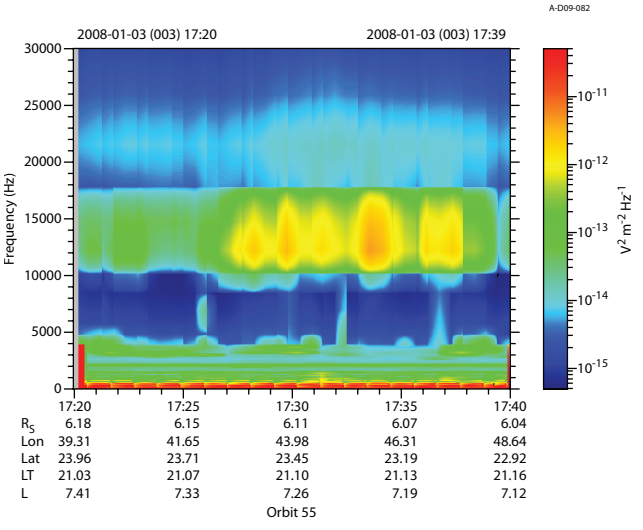

Fig. 2. A wave spectrogram showing a close up of the region near a probable source region of NB emission.

In this figure the spectral density is linearly interpolated between frequency channels producing a smoothing effect.

Circular polarization measurements for this emission as calculated from the RPWS instrument are shown in the top panel of Fig. 3 for the time interval from 16:00 to 19:00 h. In this figure, no smoothing between frequency channels is performed. Circular polarization is calculated from the three antenna direction-finding measurements of the RPWS (Cecconi and Zarka, 2005). We note that the emission centered near

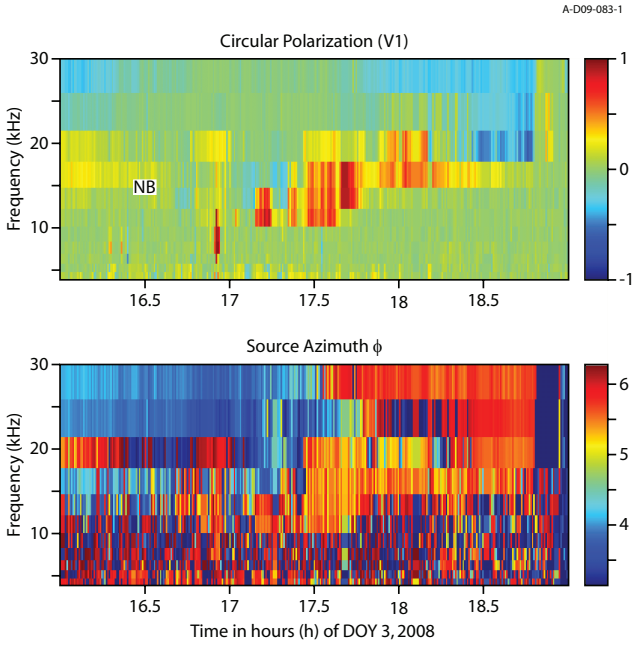

Fig. 3. Circular polarization measurements as calculated from the RPWS instrument for the time interval 16:00 to 19:00 (top panel). Near 15 kHz and 17.5 h note a transition from blue to yellow-red. The bottom panel displays the azimuth angle in radians of the direction to the source in spacecraft coordinates. A distinct change in azimuth angle occurs near 15 kHz and 17.5 h.

15 kHz has a red color (+1) corresponding to left-hand circular (LHC) polarization for times greater than about 17.5 h, but is mixed for earlier times. The polarization of O-mode emission is left-hand circular (LHC), and for $f_p/f_{ce} > 1$, the polarization of Z-mode is also LHC. The LHC polarization of Z-mode and O-mode thus appear red (+1) on the spectrogram. We interpret the transition from light blue ($V \approx -.25$) to red at ∼15 kHz near 17.5 h to indicate that the Cassini spacecraft travels through the source region thus experiencing wave vectors, $\boldsymbol{k}$, that reverse direction relative to the local magnetic field producing a reversal of the polarization. The reversal of polarization can be interpreted as evidence that the spacecraft traverses the source region. This interpretation assumes the emission wave mode does not change and is always observed from the same side of the antenna plane (the plane containing the Cassini U and V antennas, which lie in the spacecraft x-y axis). Thus the satellite is believed to have passed very near the source region.

In the bottom panel of Fig. 3 we show the azimuth angle of the direction to the source with respect to spacecraft coordinates. The color bar is in units of radians. The spacecraft orientation relative to Saturn equatorial coordinates changes very little during the time interval of Fig. 3. The importance of this panel is that it shows a rapid change of direction to the source region near 15 kHz and 17.5 h, supporting our interpretation of a spacecraft traversal of the NB source region.

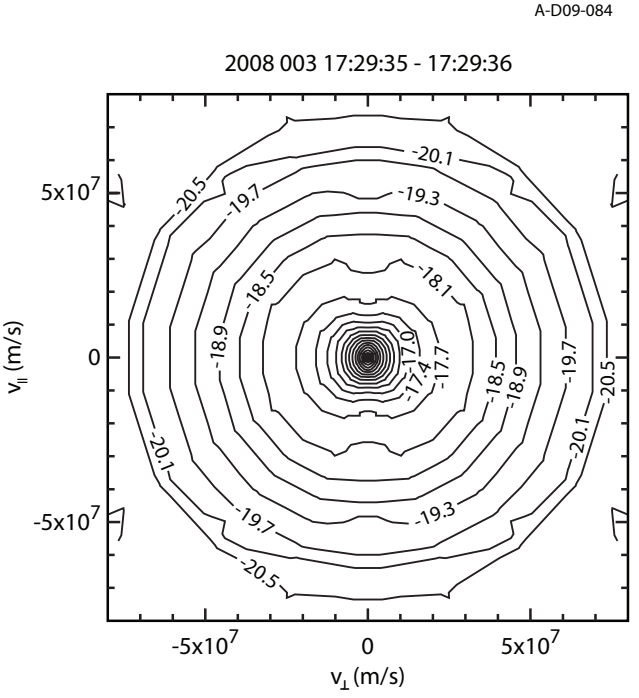

Fig. 4. Contour of the electron phase space density (PSD) for the time interval 17:29:35 to 17:29:36 for $E < 20$ keV, assuming the reflection of the data as described in the text. A loss cone for pitch angles less than about 20 degrees is observed. The contour levels are $\log_{10}$(PSD) in units of s^3/m^6.

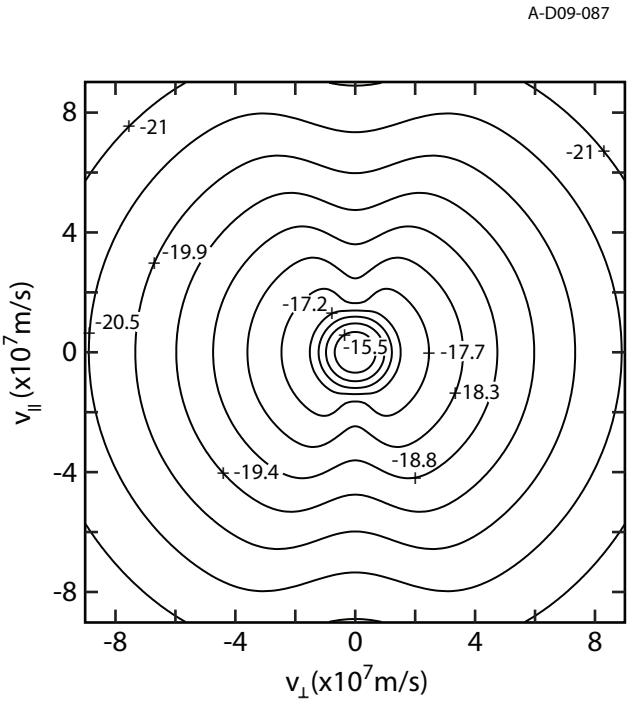

Fig. 5. Contours of PSD determined from the analytical model described by Eq. (1) with parameters from the text.

3 Growth rate calculations

Growth rate calculations for the Z and O modes require a semi-relativistic treatment. In this section we treat these emissions using an analytical approach based on the work of Yoon et al. (1996, 1998).

To investigate the generation mechanism of these waves, we require the electron phase space density (PSD) distribution. At the time of the observations, the Cassini spacecraft electron particle detector, the Electron Spectrometer (ELS), was only viewing in one hemisphere covering an approximate range of pitch angles $3.4° < \alpha < 81.4°$. Since the spacecraft is located at low L-shells ($L < 7.3$) and most probably closed field lines, we have assumed that the data are gyrotropic and can also be mirror-reflected to the supplemental range of pitch angles, $180° - \alpha$. In Fig. 4 we show a contour of the electron PSD for the time interval 17:29:35 to 17:29:36 for $E < 20$ keV, assuming the reflection of the data as described. We observe a loss cone for pitch angles less than about 20 degrees.

In order to facilitate the analytical calculation of the growth rate of Z-mode and O-mode, we introduce a functional form for the distribution function similar to that of Yoon et al. (1996) as follows:

$$f(u,\mu) = r_0 \exp\left(-\frac{u^2}{\alpha_0^2}\right) + \frac{r_e}{(1+u^2/\kappa\alpha^2)^{\kappa+1}} \cdot \left(1+\Delta-\tanh\frac{\mu^2-\mu_0^2}{\delta^2}\right) \quad (1)$$

This functional form effectively assumes a background distribution and an energetic population along with a loss cone.

The input parameters are $u = P/m_e c$ is the normalized momentum, μd = cosine of the pitch angle, $\alpha_0 = 0.02$ (parallel thermal speed for core species = 6×10^6 m/s), $r_0 = 1\times10^{-15}$ (core distribution), $\alpha = 0.0667$ (Gaussian thermal speed = 2×10^7 m/s), $\mu_0 = \cos(\theta_L) \approx 0.97$ (loss cone angle $\theta_L \approx 14°$), $\Delta = 0$ (loss cone depth factor), $\delta = 0.35$ (width of loss cone), $\kappa = 3$ (fitting parameter), $r_e = 4\times10^{-18}$ (energetic distribution).

The model distribution used in the growth rate calculation is shown in Fig. 5. The depth of the loss cone observed in the data of Fig. 4 is not precisely known since the minimum pitch angle measured is about 3.4 degrees from the magnetic field. We have chosen a model loss cone depth parameter, Δ, that produces a shallow loss cone that is unstable to the growth of the CMI.

4 Temporal and spatial growth rate

The contours of Z-mode growth rate versus propagation angle θ (in degrees) and normalized frequency ω/Ω (Ω is the

A-D09-088

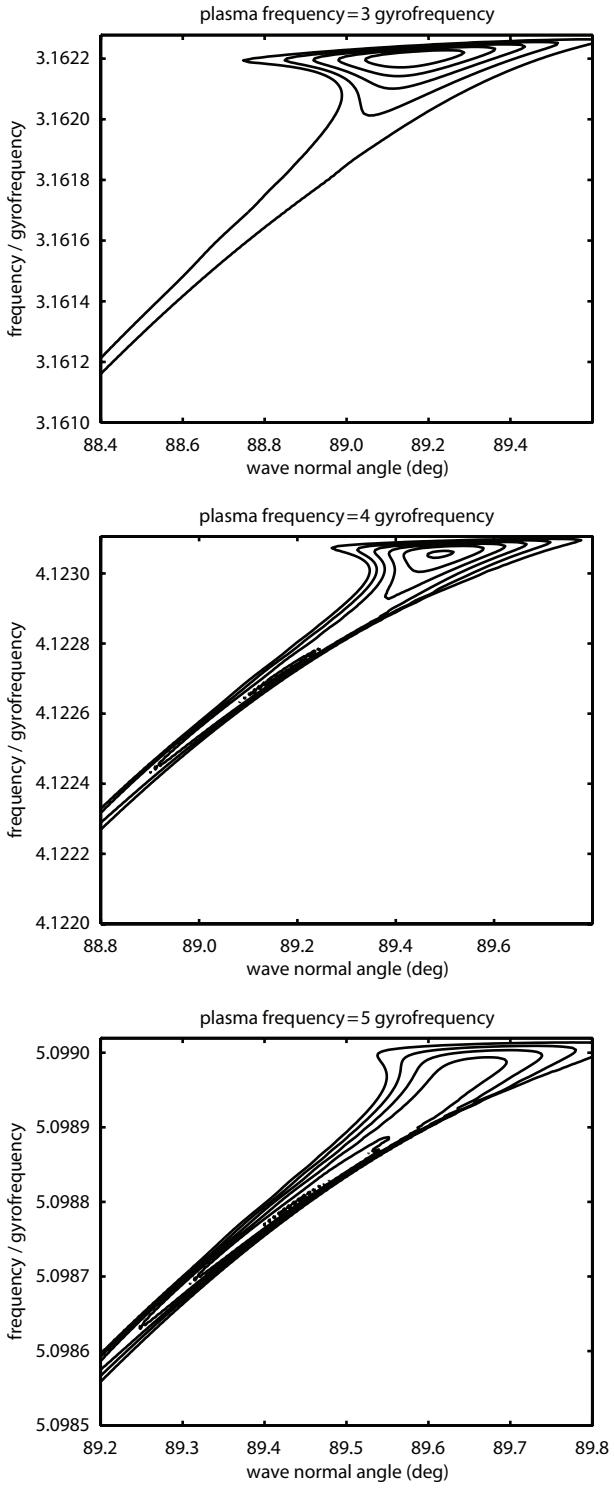

Fig. 6. Contours of the Z-mode temporal growth rate (relative to the cyclotron frequency) versus wave normal angle for three different cases of ω_p/Ω=3, 4, and 5. The peak growth rates for each panel are (top) 1.5×10^{-4}, (middle) 2.2×10^{-4}, and (bottom) 7.2×10^{-4}.

A-D09-089

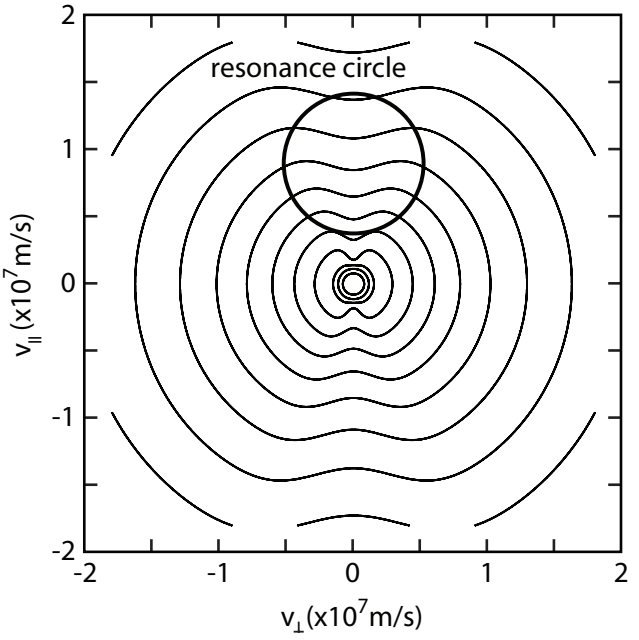

Fig. 7. Example of resonance circle for the case of ω_p/Ω=4, ω/Ω=4.123, and θ=89.5°.

cyclotron frequency) for three different cases of ω_p/Ω=3, 4, and 5 are shown in Fig. 6. An example of resonance circle in the case ω_p/Ω=4, ω/Ω=4.123, θ=89.5° is shown in Fig. 7.

We repeated the growth rate calculation for of ω_p/Ω ranging from 3 to 6 in a continuous way. For each of ω_p/Ω, we determined the most unstable mode. Most unstable modes are found to have quasi-perpendicular propagation angle, and with frequency very close to the upper hybrid frequency. Figure 8 plots the maximum growth rate γ/Ω versus ω_p/Ω. For quasi-perpendicular propagation, the relativistic resonance condition dictates that

$$\Gamma\omega - s\Omega \approx 0 \tag{2}$$

where Γ is the relativistic factor. If this factor can be approximated by unity, ω by ω_{uh}, then one can see that the resonance condition can be satisfied when

$$\frac{\omega_{uh}^2}{\Omega^2} = 1 + \frac{\omega_p^2}{\Omega^2} = s^2 \tag{3}$$

or

$$\frac{\omega_p}{\Omega} = \sqrt{s^2 - 1} \tag{4}$$

For s=4, 5, and 6 the corresponding values of ω_p/Ω are ω_p/Ω=3.8730, 4.8990, and 5.916, respectively. Z-mode growth is greatly enhanced when ω_p/Ω assumes these values. In Fig. 8, ω_p/Ω=3.8730, 4.8990, and 5.916 are indicated by arrows.

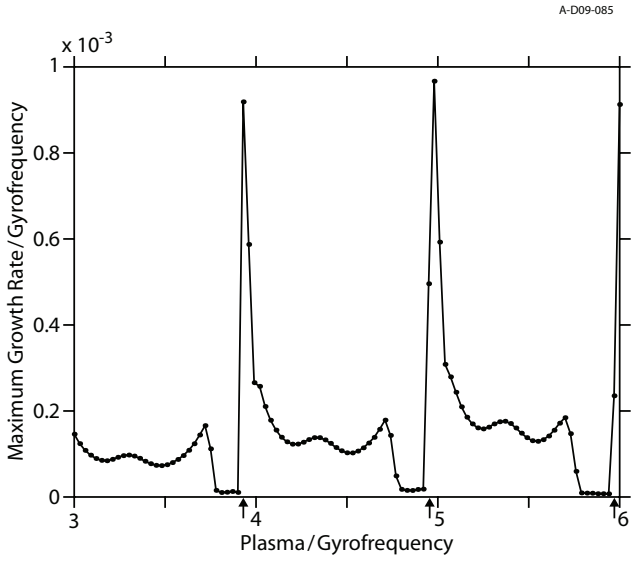

Fig. 8. Maximum Z-mode growth rate (relative to Ω) versus ω_p/Ω. The growth rate is greatly enhanced when ω_p/Ω assumes values defined by Eq. (4) of the text.

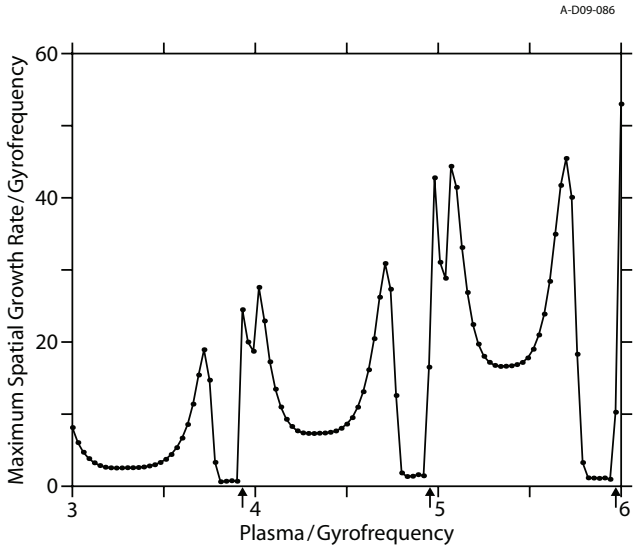

Fig. 9. Relative spatial growth rate of the Z-mode emission as a function of ω_p/Ω.

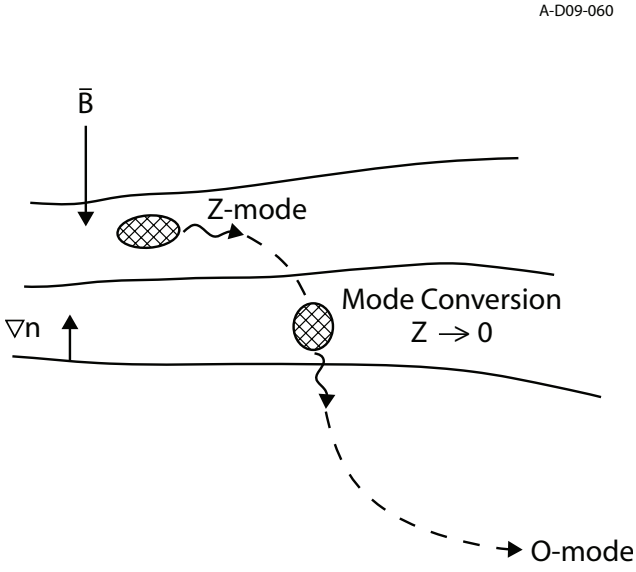

Fig. 10. A cartoon showing how Z-mode waves generated at large wave normal angles can refract to small wave normal angles in a density gradient along the magnetic field as is the case near the high latitude boundaries of the Enceladus torus. These Z-mode waves will be expected to mode convert to O-mode (NB emission) and then refract to propagate perpendicular to the density gradient.

The results indicate a narrow bandwidth associated with the condition f_{uh}=nf_{ce}. To explain the bandwidth of intense emission shown in Fig. 2, extending from about 10 kHz to about 17.5 kHz, we hypothesize emission occurs within a region of strong density gradient that contains a range of plasma densities, ∼9 kHz< f_p <∼ 17.5 kHz while the spacecraft position changes over the time interval 17:26 to 17:39.

In Fig. 9 we plot the relative spatial growth of the Z-mode emission as a function of ω_p/Ω. The spatial growth is the temporal growth rate divided by v_g/c, where v_g is the group velocity and c is the speed of light. For $\omega_p/\Omega \sim 5$ we find the maximum spatial growth approaches 45.

The convective growth length, L_c=v_g/ω_i, where ω_i is the imaginary frequency. From Fig. 9 we find $\omega_i c/v_g$=45, and Fig. 8 indicates $\omega_i \sim 1.0\times10^{-3}\Omega$, giving v_g=.436 c and $L_c \sim 6.5\times10^3$ km.

It is well known that the cold plasma formulation for the index of refraction, N, for the Z and O modes are nearly coincident under certain conditions (cf. Stix, 1992; Benson et al., 2006). For instance, the curves for N^2 versus ω nearly intersect for wave normal angles <2° and $\omega_p/\Omega \sim 4$. For $\omega > 4\Omega$, $N > 1$, and Z-mode waves generated at large wave normal angles will refract to small wave normal angles in a density gradient along the magnetic field as is the case near the high latitude boundaries of the Enceladus torus. These Z-mode waves will be expected to mode convert to O-mode and then refract to propagate perpendicular to the density gradient. This process is shown schematically in Fig. 10.

In Fig. 1 we have indicated another possible source region of NB emission near 18:55 UT. This source region is associated with a higher density but lower temperature. Polarization measurements shown in Fig. 3 do not aid us for this time period, because the spacecraft began a 90° roll movement starting at about 18:50 UT continuing to about 19:10 UT. It is extremely difficult to interpret the change in color seen in Fig. 3 above 20 kHz near 18.8 h from blue to yellow. The change can be due to passage through the source region and/or to the rotation of the spacecraft. The electron

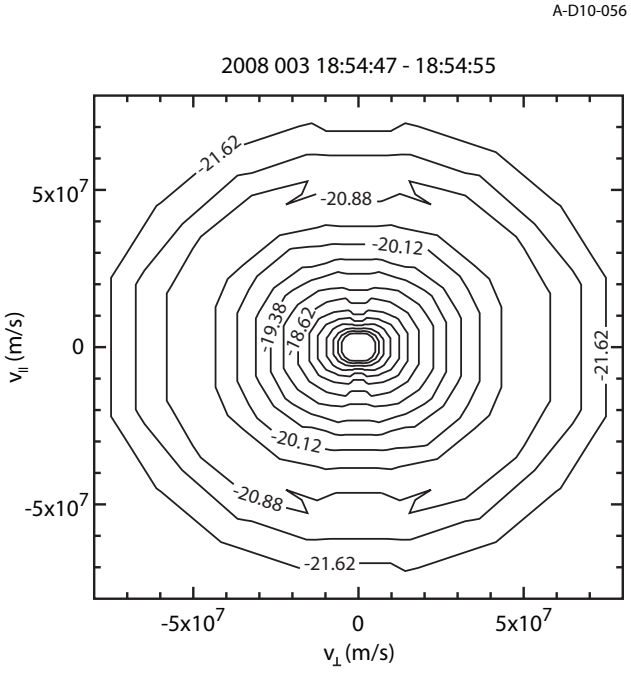

Fig. 11a. Contours of the electron phase space density for the period 18:54:47 to 18:54:55 in the same format as Fig. 4.

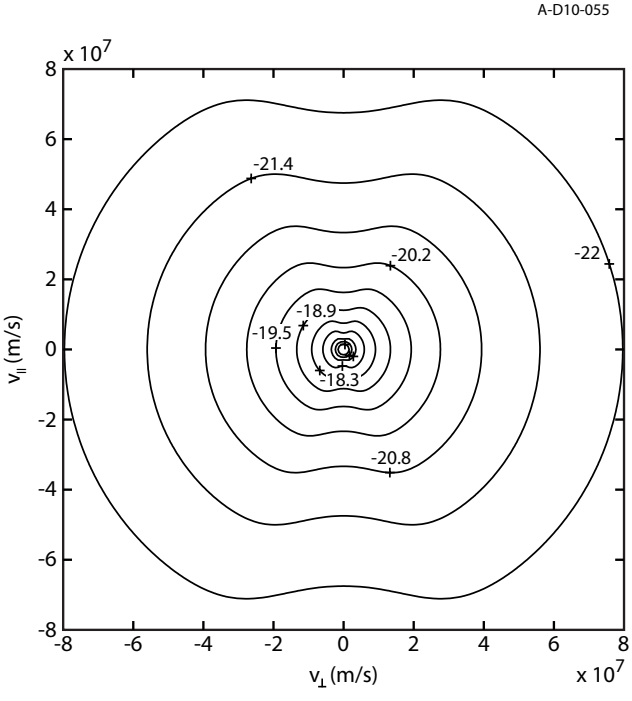

Fig. 11b. Contours of the PSD determined from the analytical model described by Eq. (1), but now using parameters for the event of Fig. 11a.

distribution for the time period 18:54:47–18:54:55 is shown in Fig. 11a, which can be compared to Fig. 4. Note that the distribution of Fig. 11a was collected over a longer period

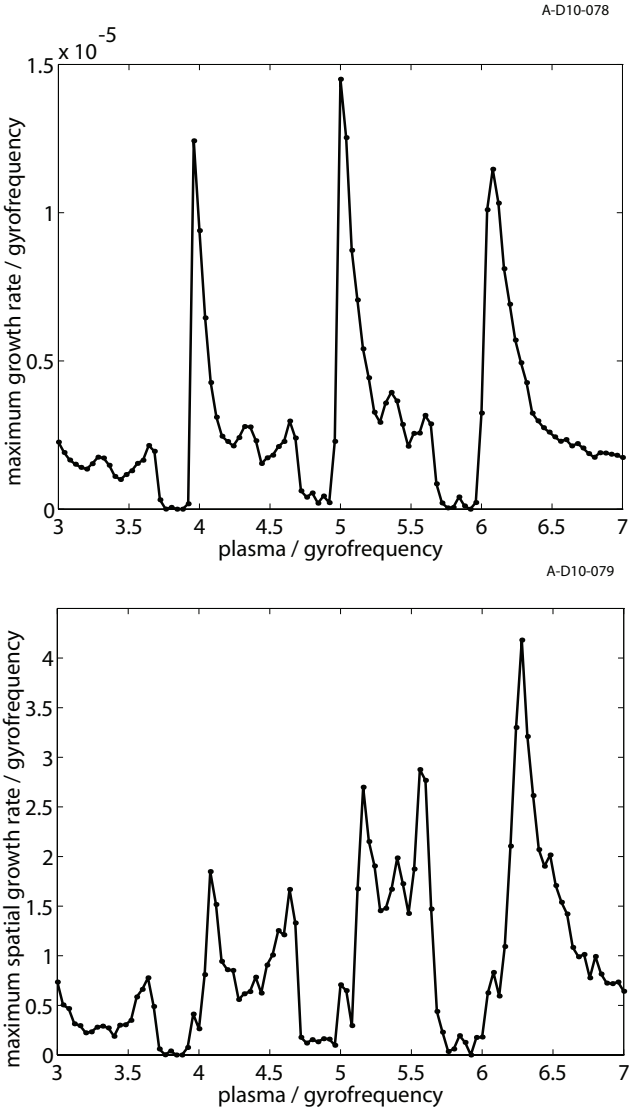

Fig. 12. Calculated values of Z-mode temporal growth rate relative to Ω **(a)** and spatial growth rate **(b)** versus ω_p/Ω, but now for the probable source near 18:55 UT.

due to the operational mode of the ELS instrument. Importantly, a loss cone is observed in the distribution shown in Fig. 11a similar to that shown in Fig. 4. However, for the data collected in Fig. 11a the smallest observed pitch angle is ∼7.5° (compared to ∼3.4° for Fig. 4). We have conducted a growth rate analysis for this new distribution as before. The model distribution function is again given by Eq. (1), but now with

$\alpha_0 = 0.0043$ (parallel thermal speed for core species = 1.30×10^6 m/s)

$\alpha = 0.0115$ (Gaussian thermal speed = 9.19×10^6 m/s)

$\kappa = 1$

$r_0 = 5 \times 10^{-16}$ (core distribution)

$r_e = 1 \times 10^{-17}$ (energetic distribution)

The model distribution is shown in Fig. 11b.

The loss cone parameters are the same as before. Even though the overall density of this distribution is somewhat higher, the temperature is lower, leading to a lower value of kappa, and smaller growth rates, as displayed in Fig. 12. This figure has the same format as Figs. 8 and 9 but includes one higher harmonic. As seen by comparison, the temporal growth rates for Z-mode shown in Fig. 12 are positive and occur for wave normal angles $>88°$, but they are almost 2 orders of magnitude lower than those shown in Fig. 8. The spatial growth rates shown in Fig. 12 are only about 1 order of magnitude smaller, yielding a large convective growth length of 7.1×10^4 km. This weak growth may be due to a relaxed electron distribution due to instrumental limitations. It is certainly possible that the loss cone observed at this time is much steeper and deeper, because there are no observations for the smallest pitch angles ($<7.5°$ at this time), and the distribution required a number of seconds to collect.

5 Discussion and summary

Next to Saturn kilometric radiation, Saturn NB emission is perhaps among the more common and intense of the radio emissions observed at Saturn. In this study we have isolated two examples of this emission at ∼14 kHz and ∼20 kHz near a fortuitous encounter by Cassini of a probable source region, and we study the occurring generation mechanisms. We have been fortunate to obtain electron phase space densities with a sufficient pitch angle distribution for analysis. The results reported here support and extend the work of Menietti et al. (2009).

We use the theory of the cyclotron maser instability and a tractable analytic model of the electron distribution function (Eq. 1 and Fig. 5) to calculate the wave temporal and spatial growth rate for both Z-mode and O-mode (NB) emission. This is possible because, as discussed by Yoon et al. (1998) when the local upper hybrid frequency is in close vicinity to $n\Omega$, harmonic Z-mode emission growth rate can be exceedingly high. Our results indicate that the Z-mode emission has a peak growth rate that is many orders of magnitude larger than the O-mode (Fig. 6), and a convective growth length of about 6500 km. To account for the observed O-mode emission seen in Figs. 1 and 2 (NB), we postulate a mode conversion from Z-mode to O-mode near the satellite location during the interval 17:26 to 17:39 UT. Using the measured plasma parameters for this event in cold plasma theory we find that the dispersion curves for the Z-mode and O-mode are nearly coincident for a wave normal angle less than 2° for each mode. These results therefore indicate that a likely source of the observed NB emission is mode conversion of Z-mode to O-mode near the density gradient (indicated by the falling magnitude of f_{UH} seen in Fig. 1) where the index of refraction of the two modes match.

Growth rate calculations for the possible source near 18:55 produce only weak growth of Z-mode emission, even though the observed NB emission for this source region appears just as intense in Fig. 1 as the emission from the source near 17:30 UT. While we believe that the same growth mechanism for Z-mode emission followed by mode conversion to O-mode is taking place for both source regions, there is evidence that the measured electron distribution function may be relaxed, thus explaining the small calculated growth rates. Another source of Z-mode emission may be linear or nonlinear conversion of upper hybrid waves near a steep density gradient as discussed earlier (cf. Jones, 1976; Melrose, 1981).

The Saturn NB emission is similar in morphology to terrestrial continuum emission and to Jovian nKOM emission (Louarn et al., 2007), implying that the analysis presented may have feasibility at other planets. Recent evidence indicates that NB emission near 5 kHz has a different source region than NB emission near 20 kHz (cf. Ye et al., 2009). Future studies of the source region and generation of this emission will be important.

Acknowledgements. We thank J. Barnholdt and K. Kurth for clerical assistance. This research was supported by NASA through Jet Propulsion Laboratory contract 1356500 with the University of Iowa. PHY acknowledges NSF grant ANT 0838647 to the University of Maryland and WCU grant No. R31-10016 from the Korean Ministry of Education, Science and Technology to the Kyung Hee University. We thank A. J. Coates for providing the ELS data in a useable format.

Topical Editor R. Nakamura thanks P. H. M. Galopeau and another anonymous referee for their help in evaluating this paper.

References

Barbosa, D. D.: Low-level VLF and LF radio emissions observed at Earth and Jupiter, Rev. Geophys., 20, 316–334, 1982.

Benson, R. F., Webb, P. A., Green, J. L., Carpenter, D. L., Sonwalkar, V. S., James, H. G., and Reinisch, B. W.: Active wave experiments in space plasmas: The Z mode, in: Geospace Electromagnetic Waves and Radiation, edited by: LaBelle, J. W. and Treumann, R. A., Springer, Berlin, 2006.

Budden, K. G.: The theory of radio windows in the ionosphere and magnetosphere, J. Atmos. Terr. Phys., 42(3), 287–298, 1980.

Cecconi, B. and Zarka, P.: Direction finding and antenna calibration through analytical inversion of radio measurements performed using a system of two or three electric dipole antennas on a three-axis stabilized spacecraft, Radio Sci., 40, RS3003, doi:10.1029/2004RS003070, 2005.

Ellis, G. R.: The Z propagation hole in the ionosphere, J. Atmos. Terr. Phys., 8, 43–54, 1956.

Fung, S. F. and Papadopoulos, K.: The emission of narrow-band Jovian kilometric radiation, J. Geophys. Res., 92, 8579–8593, 1987.

Gurnett, D. A.: The earth as a radio source: The nonthermal continuum, J. Geophys. Res., 80, 2751–2763, 1975.

Gurnett, D. A. and Shaw, R. R.: Electromagnetic radiation trapped in the magnetosphere above the plasma frequency, J. Geophys. Res., 78, 8136–8149, 1973.

Gurnett, D. A., Kurth, W. S., and Scarf, F. L.: Narrowband electromagnetic emissions from Saturn's magnetosphere, Nature, 292, 733–737, 1981.

Gurnett, D. A., Kurth, W. S., and Scarf, F. L.: Narrowband electromagnetic emissions from Jupiter's magnetosphere, Nature, 302, 385–388, 1983.

Horne, R. B.: Path-integrated growth of electrostatic waves: The generation of terrestrial myriametric radiation, J. Geophys. Res., 94, 8895–8909, 1989.

Horne, R. B.: Narrow-band structure and amplitude of terrestrial myriad-metric radiation, J. Geophys. Res., 95, 3925–3932, 1990.

Jones, D.: Source of terrestrial non-thermal continuum radiation, Nature, 260, 686–689, 1976.

Jones, D.: Planetary radio emissions from low magnetic latitudes: Observations and theories, in: Planetary Radio Emissions II, edited by: Rucker, H. O., Bauer, S. J., and Pedersen, B.-M., pp. 255–293, Austrian Academy of Science Press, Graz, Austria, 1988.

Kurth, W. S.: Continuum radiation in planetary magnetospheres, in: Planetary Radio Emissions III, edited by: Rucker, H. O., Bauer, S. J., and Kaiser, M. L., pp. 329–350, Austrian Academy of Science, 1992.

Kurth, W. S., Ashour-Abdalla, M., Frank, L. A., Kennel, C. F., Gurnett, D. A., Sentman, D. D., and Burek, B. G.: A comparison of intense electrostatic waves near f_{UHR} with linear instability theory, Geophys. Res. Lett., 6, 487–490, 1979a.

Kurth, W. S., Craven, J. D., Frank, L. A., and Gurnett, D. A.: Intense electrostatic waves near the upper hybrid resonance frequency, J. Geophys. Res., 84, 4145–4164, 1979b.

Louarn, P., Kurth, W. S., Gurnett, D. A., et al.: Observations of similar radio signatures at Saturn and Jupiter: Implications for the magnetospheric dynamics, Geophys. Res. Lett., 34, L20113, doi:10.1029/2007GL030368, 2007.

Melrose, D. B.: A theory for the nonthermal radio continua in the terrestrial and Jovian magnetospheres, J. Geophys. Res., 86, 30–36, 1981.

Menietti, J. D., Ye, S.-Y., Yoon, P. H., Santolik, O., Rymer, A. M., Gurnett, D. A., and Coates, A. J.: Analysis of narrowband emission observed in the Saturn magnetosphere, J. Geophys. Res., 114, A06206, doi:10.1029/2008JA013982, 2009.

Morgan, D. D. and Gurnett, D. A.: The source location and beaming of terrestrial continuum radiation, J. Geophys. Res., 86, 9595–9613, 1991.

Ronnmark, K.: Emission of myriametric radiation by coalescence of upper hybrid waves with low frequency waves, Ann. Geophys., 1, 187–192, 1983.

Ronnmark, K.: Myriametric radiation and the efficiency of linear mode conversion, Geophys. Res. Lett., 16, 731–738, 1989.

Ronnmark, K.: Conversion of upper hybrid waves into magnetospheric radiation, in: Planetary Radio Emissions III, edited by: Rucker, H. O., Bauer, S. J., and Kaiser, M. L., p. 405, Austrian Academy of Science, Graz, Austria, 1992.

Ronnmark, K., Borg, H., Christiansen, P. J., Gough, M. P., and Jones D.: Banded electron cyclotron harmonic instability–A first comparison of theory and experiment, Space Sci. Rev., 22, 401–417, 1978.

Scarf, F. L., Gurnett, D. A., Kurth, W. S., and Poynter, R. L.: Voyager 2 plasma-wave observations at Saturn, Science, 215, 587–594, 1982.

Stix, T. H.: Waves in Plasmas, pp. 556, American Institute of Physics, New York, 1992.

Wang, Z., Gurnett, D.A., Fischer, G., Ye, S.-Y., Kurth, W. S., Mitchell, D. G., Leisner, J. S., and Russell, C. T.: Cassini observations of narrowband radio emissions in Saturn's magnetosphere, J. Geophys. Res., in press, 2010.

Wu, C. S. and Lee, L. C.: A theory of terrestrial kilometric radiation, Astrophys. J., 230, 621–626, 1979.

Ye, S., Gurnett, D. A., Fischer, G., Cecconi, B., Menietti, J. D., Kurth, W. S., Wang, Z., Hospodarsky, G. B., Zarka, P., and Lecacheux, A.: Source location of narrowband radio emissions detected at Saturn, J. Geophys. Res., 114, A06219, doi:10.1029/2008JA013855, 2009.

Yoon, P. H., Weatherwax, A. T., Rosenberg, T. J., and LaBelle, J.: Lower ionospheric cyclotron maser theory: A possible source of $2f_{\mathrm{ce}}$ and $3f_{\mathrm{ce}}$ auroral radio emissions, J. Geophys. Res., 101, 27015–27025, 1996.

Yoon, P. H., Weatherwax, A. T., Rosenberg, T. J., LaBelle, J., and Shepherd, S. G.: Propagation of medium frequency (1-4 MHz) auroral radio waves to the ground via the Z-mode radio window, J. Geophys. Res., 103, 29267–29275, 1998.